Eur. Phys. J. E **1**, 179–188 (2000)

THE EUROPEAN PHYSICAL JOURNAL E

EDP Sciences
© Società Italiana di Fisica
Springer-Verlag 2000

Interface dynamics in liquid crystals

C. Chevallard, M. Clerc[a], P. Coullet, and J.-M. Gilli

Institut Non-Linéaire de Nice[b], 1361 route des Lucioles, 06560 Valbonne, France

Received 5 August 1999 and Received in final form 13 September 1999

Abstract. We have experimentally observed the pattern instabilities of an Ising wall formed in a nematic or cholesteric liquid crystal layer. We have deduced an envelope equation, relevant close to the Fréedericksz transition, from which we derived an equation for the dynamics of the interface in the vicinity of its bifurcation. In the case of the zig-zag instability, this model is characterized by a conservative and variational order parameter whose gradient satisfies a Cahn-Hilliard equation. We have also investigated the influence of slightly broken symmetries on the dynamical behaviour of the system. The disappearance of the interface translational invariance or of the reflection symmetry along the wall axis may induce new interfacial patterns which have been both experimentally and theoretically pointed out.

PACS. 47.20.Ma Interfacial instability – 47.20.Ky Nonlinearity (including bifurcation theory) – 61.30.Gd Orientational order of liquid crystals; electric and magnetic field effects on order

1 Introduction

Interfacial instabilities and pattern formation have stimulated a great deal of study during recent decades. In most cases, the interface is a moving boundary between two different states. For example, in the problem of crystal growth, rich morphological instabilities may arise from the destabilization of the solidification front (see [1] for a specific review and [2] more generally). Two kinds of solidification processes are generally distinguished [1]. In one of them, the crystal freely grows up from its undercooled melt, whereas in the so-called directional growth, the solidification is forced by drawing the liquid sample across a linear thermal gradient. Many of the observed instabilities and interfacial patterns are actually common to these two situations. In both cases, the smooth interface (planar or circular) may undergo a spatial instability (Mullins and Sekerka's instability [3]) for a sufficiently high solidification rate. In free growth, this instability is controlled by the undercooling degree of the melt. Beyond the instability threshold, a dendritic pattern arises in the system [4,5]; due to the secondary tip-splitting and sidebranching instabilities, this pattern may evolve towards a strongly disordered even fractal form (as for example in the formation of snowflakes). In directional growth, the instability is governed by the pulling speed value and leads first to a cellular pattern [6]. Starting form a cellular interface, one can, by increasing the sample velocity, induce successive instabilities that are tip-splitting, period-halving, fingering, and lastly dendritic instabilities [7]. By further increasing the pulling speed, one enters the kinetics-controlled regime [7] where the out-of-equilibrium front may exhibit highly complex behaviours.

The analysis of the forces which act on the interface shows in both situations that the process which drives the destabilization of the front is predominantly diffusive (either thermal or chemical diffusion) [1]. The competing stabilizing force is the capillary force which prevents the front from an irregular growth. In directional solidification, one must take into account another stabilizing effect due to the thermal gradient (it acts as a restoring force around the position corresponding to the melting temperature [8,9]). This accounts for the cellular pattern emerging beyond the Mullins and Sekerka instability. The directional fingers, that can be observed in this situation, are very similar [10] to those which appear in the Saffman-Taylor problem [11]. There, an instability may affect the straight moving boundary between two viscosity-contrasted fluids, when one pushes the less viscous fluid into the other one by use of a pressure gradient applied at the edges of a porous medium or of a Hele-Shaw cell. The destabilizing and stabilizing forces are respectively the viscous and capillary forces.

Numerous other examples of interface destabilization and interfacial patterns could be enumerated. In the field of liquid crystals, the interface between nematic and isotropic phases or between distorted and undistorted regions of the nematic phase can exhibit interesting dynamical behaviours [12]. In purely elastic problems, the orientational dynamics of liquid crystals is variational since it derives from a free energy (Frank energy). Within this context, we shall consider in this work an interface that separates two symmetrical, energetically equivalent states

[a] e-mail: clerc@inln.cnrs.fr
[b] UMR 6618 CNRS-UNSA

of the liquid crystal phase. We shall see that this property results in new dynamical behaviours for the interface.

In all cases, provided that the interface can be treated as a one-dimensional system whose dynamical behaviour allows a local description, one can characterize its temporal evolution by a unique scalar order parameter P (in directional growth, the previous assumptions are only verified in the kinetics-controlled regime, *i.e.* for very high velocities of the front [7]). More precisely P defines the position of the interface. In the case of a planar interface, the general symmetries to be considered are the translational invariance of the interface ($P \longrightarrow P + P_0$) and the space reflection symmetry in the direction tangent to the interface ($y \longrightarrow -y$). When the flat interface is stable, the order parameter satisfies asymptotically the following nonlinear diffusion equation

$$\partial_t P = \varepsilon P_{yy} \pm P_y^2 \,, \qquad (\varepsilon \sim O(1)). \tag{1}$$

The nonlinearity corresponds to an advective term along the interface. Introducing the change of variable $v = P_y$ into the previous equation leads to the Burgers equation [13]. The nonlinear term is responsible for the displacement of the front in the direction perpendicular to itself. For the sake of simplicity we shall suppose that it is positive. Then a small perturbation that locally moves the interface forward, is advected along the front by the nonlinear term and so grows up. Whereas the same perturbation in the opposite direction vanishes due to the advection. The sum of these two effects results in the motion of the interface.

When ε becomes small (positive or negative), the interface dynamics is generally modelled by the new asymptotic non-variational equation:

$$\partial_t P = \varepsilon P_{yy} + P_y^2 - P_{yyyy} \tag{2}$$

which is the well-known Kuramoto-Sivashinsky equation [14,15]. It gives the dynamical behaviour of the interface in the vicinity of the bifurcation. It has been derived by Sivashinsky to describe the diffusive instabilities of planar flame fronts [15,16]. It has been concurrently established by Kuramoto [14] within the framework of phase dynamics in reaction-diffusion systems. This equation provides a good model for free solidification at large supercooling [17] as well as for free faceted solidification (due to the crystal anisotropy) of a pure substance [18]. In this latter work, the new nonlinear diffusion term $P_y^2 P_{yy}$ is added in order to account for the faceting phenomenon. The Kuramoto-Sivashinsky equation exhibits spatio-temporal chaotic behaviours [19] and supplies an accurate description for phase turbulence in chemical systems [20] and for turbulent flame fronts [16]. Finally, the equation (2) with an extra linear damping term shows spatio-temporal intermittency and reproduces [8] quite well some of the kinetics-controlled behaviours observed [21] in directional crystal growth (the damping term expresses the loss of translational invariance due to the thermal gradient).

When the interface separates two symmetrical states, one must take into account a third symmetry which is the space reflection in the direction normal to the interface ($x \rightarrow -x$). In consequence the Kuramoto-Sivashinsky model has to be abandoned. If the interface is stable, the dynamics is now given by a simple diffusion equation. Perturbations relax without any change on the interface position. When the diffusion coefficient goes to zero, the nonlinear term must be replaced by the nonlinear diffusion term $P_y^2 P_{yy}$ in the fourth-order derivative equation. This latter has a variational form and constitutes a continuity equation that expresses the conservation of the order parameter integral [22]. It is similar to the equation which describes the "zig-zag" instability for the phase in the structures of straight rolls in the Rayleigh-Bénard problem [23] or in the electroconvection of anisotropic fluids [24].

In this paper we first propose a brief introduction to liquid crystals and then present the set-up (see Sect. 2) that has been used for all experiments on these complex fluids. In Section 3, we derive a model from physical mesoscopic equations to explain the zig-zag like instability that affects a splay-bend Ising wall formed in a nematic liquid crystal film. This zig-zag instability and the subsequent coarsening dynamics are both experimentally and theoretically characterized. The following section (Sect. 4) underlines the influence of a translational symmetry-breaking on the interface dynamical behaviour. Experimentally this situation is reached by applying a magnetic field gradient to the sample, which localizes the interface around a specific position. Finally the case of a reflection symmetry-breaking along the interface axis is considered in Section 5. As we shall see, such a situation can be encountered experimentally by using a cholesteric liquid crystal sample instead of a nematic one.

2 Liquid crystal experiments

Liquid crystal fluids are made of anisotropic-shaped organic molecules. This results in a strong anisotropy of all their physical properties, especially optical properties. In the nematic phase, the configuration of lowest energy is reached when all the rod-like molecules are aligned along one averaged direction denoted by a vector $\mathbf{n}$, which is called the director (any description must include the symmetry $\mathbf{n} \leftrightarrow -\mathbf{n}$). This direction can be specified either by applying an external field, like an electric or magnetic field, or by imposing some particular boundary conditions (anchoring conditions) at the edges of the confined sample. When two of these constraints are competing, the long-range orientational order may be partially destroyed. Orientational deformations then appear in the system. These are theoretically described by a vector field $\mathbf{n}(\mathbf{r}, t)$ which indicates the averaged orientation of the molecules in the fluid particle located in $\mathbf{r}$. This phenomenon actually occurs when one tries to induce the reorientation of the molecules, thanks to an external field, in an anchored layer of nematic liquid crystal. For a sufficiently high magnitude of the field, the initial alignment, due to the anchoring, is suppressed in the bulk. This is the so-called Fréedericksz instability [25]. Owing to the twofold degeneracy of the bifurcated state, domains of opposite (re-)orientation may

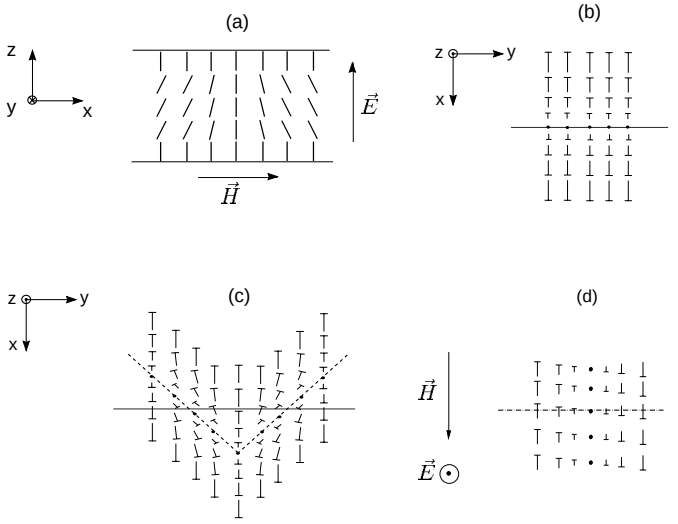

Fig. 1. Director field inside the wall: (a) and (b) splay-bend Ising wall; (c) zig-zag wall; (d) twist wall.

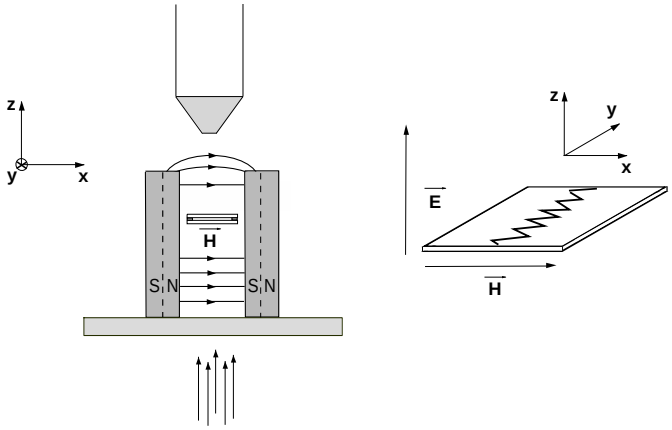

Fig. 2. Experimental set-up: the sample of liquid crystal is placed between two permanent magnets which determine the homogeneous magnetic field **H**. The physical phenomena are observed through a polarizing microscope.

be created as shown in Figure 1a [26]. The interface between two of these domains is called an Ising wall in the homeotropic geometry of the Fréedericksz transition [27] (*cf.* Figs. 1a and 1b; in this geometry the molecules are anchored perpendicularly to the boundary glass plates). Thus the Ising wall is a topological defect of the Fréedericksz bifurcation [28].

When an Ising wall is formed in a liquid crystal with a *negative anisotropy of dielectric susceptibility*, submitted both to a horizontal magnetic field and to a vertical electric field, one can destabilize it by changing the amplitude of the fields. The Ising wall becomes then a Bloch wall [28]. This instability is explained by the appearance of a second marginal mode in the vicinity of the Fréedericksz bifurcation.

In the experiments we have used liquid crystals with a *positive anisotropy of dielectric susceptibility*; then the previous instability cannot happen since there exists a unique marginal mode in the neighbourhood of the Fréedericksz transition. In this case, we shall see both experimentally and theoretically that a new kind of instability for the Ising wall may occur, that is a "zig-zag" like instability [22]. This arises because of the elastic anisotropy of the liquid crystal, that is the difference in the energetic cost of the various orientational deformations, often called *elastic distortions*. Such an instability has also be noticed to modify the form of the rolls in convection problems [23,24] whereas in crystal growth it affects the front between the two competing thermodynamic phases [18].

In the experiments we used a cyanobiphenyl compound (5CB) which is in a nematic phase at room temperature. Its anisotropic physical properties are well-characterized by the following constants, at $T = 25$ °C: elastic constants $K_1 = 6.3$, $K_2 = 4.1$, $K_3 = 8.4$ ($\times 10^{-7}$ dynes); dielectric anisotropy $\epsilon_a = 11.3$; diamagnetic anisotropy $\chi_a = 1.142$ ($\times 10^{-7}$ cm^3 g^{-1}); rotational viscosity $\gamma_1 \sim 10^{-2}$ Pa s.

The samples are made of two glass plates separated by thin mylar spacers which determine the width of the cell (between 50 and 250 μm). The glass surfaces are treated with lecithin to provide a homeotropic anchoring (molecules perpendicular to the plates). The sample is subjected to a sinusoidal vertical electric field $\mathbf{E} = E\mathbf{e}_z$ ($V_{\text{eff}} \sim 0{-}9$ V) with a high frequency (~ 5 kHz) in order to avoid charge injection or electroconvection phenomena. Moreover, two permanent magnets produce a horizontal magnetic field near the sample. The field magnitude can be changed by moving the magnets nearer or farther. Its value is about 0.5 tesla. Here the Fréedericksz transition is induced by the magnetic field, whereas the electric field stabilizes the initial homeotropic state. An Ising wall in a splay-bend configuration [27] is formed by using the curvature of the flux lines in a region where the field is inhomogeneous (see Fig. 2). Its width is determined by the distance to the threshold of the Fréedericksz transition and can be modified by variations of the fields magnitude.

All the experimental observations are made by using a polarizing microscope (see Fig. 2). Video films or numerical images (see Figs. 3 and 4) can be registered thanks to a 3 CCD camera placed on the top of the microscope.

3 Zig-zag instability of an Ising wall in nematic liquid crystals

The experiments have been realized far from the Fréedericksz transition, since close to this one any experimental imperfection is amplified. However, we shall derive the theoretical model in the vicinity of the Fréedericksz transition, since in this limit analytical results are accessible. From this model, one can identify the physical mechanisms that give rise to the instabilities, and make a qualitative comparison with the experiments.

In the vicinity of the Fréedericksz transition the molecules are weakly tilted from the z-axis. Within this context, it is reasonable to neglect backflow effects in the

bulk. The dynamical equation for the director $\mathbf{n}$, reads [25]

$$\begin{aligned}\gamma_1\partial_t\mathbf{n} = {} & K_3\left[\nabla^2\mathbf{n} - \mathbf{n}\left(\mathbf{n}\cdot\nabla^2\mathbf{n}\right)\right] \\ & + (K_3-K_1)\left[\mathbf{n}\left(\mathbf{n}\cdot\boldsymbol{\nabla}\right)\left(\boldsymbol{\nabla}\cdot\mathbf{n}\right) - \boldsymbol{\nabla}\left(\mathbf{n}\cdot\boldsymbol{\nabla}\right)\right] \\ & + (K_2-K_3)\,2\left[\left(\mathbf{n}\cdot\boldsymbol{\nabla}\times\mathbf{n}\right)\left(\mathbf{n}\left(\mathbf{n}\cdot\boldsymbol{\nabla}\times\mathbf{n}\right) - \boldsymbol{\nabla}\times\mathbf{n}\right)\right. \\ & \left. + \mathbf{n}\times\boldsymbol{\nabla}\left(\mathbf{n}\cdot\boldsymbol{\nabla}\times\mathbf{n}\right)\right] + \chi_{\mathrm{a}}\left(\mathbf{n}\cdot\mathbf{H}\right)\left(\mathbf{H}-\mathbf{n}\left(\mathbf{n}\cdot\mathbf{H}\right)\right) \\ & + \epsilon_{\mathrm{a}}\left(\mathbf{n}\cdot\mathbf{E}\right)\left(\mathbf{E}-\mathbf{n}\left(\mathbf{n}\cdot\mathbf{E}\right)\right). \end{aligned} \tag{3}$$

The homeotropic state ($\mathbf{n} = \hat{\mathbf{z}}$) undergoes a stationary instability for critical values of the horizontal magnetic field ($\mathbf{H} = H\hat{\mathbf{x}}$) and vertical electric field ($\mathbf{E} = E\hat{\mathbf{z}}$) which satisfy the relation $-\epsilon_{\mathrm{a}}E^2 - K_3\pi^2/d^2 + \chi_{\mathrm{a}}H^2 = 0$. The first Fourier mode of the x-component of the director is then unstable ($n_x = Z(t)\cos(\pi z/d)$), and satisfies the following equation

$$\gamma_1\partial_t Z = \varepsilon Z - bZ^3 + \left(K_1\partial_x^2 + K_2\partial_y^2\right)Z \tag{4}$$

where

$$\varepsilon \equiv -\epsilon_{\mathrm{a}}E^2 - K_3\frac{\pi^2}{d^2} + \chi_{\mathrm{a}}H^2,$$

and

$$b \equiv \frac{1}{2}\left(K_1 - \frac{3}{2}K_3\right)\frac{\pi^2}{d^2} - \frac{3}{4}\left(\epsilon_{\mathrm{a}}E^2 - \chi_{\mathrm{a}}H^2\right).$$

The latter equation is the Landau equation which describes the dynamics of domains. Here these are orientational domains since beyond the Fréedericksz instability, the molecules in the bulk can be tilted in two equivalent directions. The preceding equation exhibits Ising wall solutions (splay-bend or twist wall). The splay-bend wall (see Fig. 1b) is perpendicular to the magnetic field and is a solution of the form:

$$Z_{\mathrm{sb}} = \pm\sqrt{\frac{\varepsilon}{b}}\tanh\left(\sqrt{\frac{\varepsilon}{2K_1}}\left(x - x_0\right)\right). \tag{5}$$

The twist wall (see Fig. 1d) is parallel to the magnetic field and is described by:

$$Z_{\mathrm{t}} = \pm\sqrt{\frac{\varepsilon}{b}}\tanh\left(\sqrt{\frac{\varepsilon}{2K_2}}\left(y - y_0\right)\right). \tag{6}$$

If the elastic restoring torque does not depend on the involved distortions (isotropic torque, $K_1 = K_2$), then the two last walls are energetically equivalent. In this case, any structure obtained from a spatial rotation of the splay-bend solution is again a wall-type solution of the equation (4), with the same free energy per unit length [27].

In the derivation of the previous equation we assumed that all the elastic constants are of order one, using therefore the simple asymptotic limit $Z \sim \varepsilon^{1/2}$, $\partial_y^2 \sim \partial_x^2 \sim \varepsilon$, $K_1 \sim K_3 \sim 1$, and $K_2 \sim 1$. However, in this asymptotic limit, the splay-bend Ising walls are stable. With such a limit, one cannot explain the zigzag instability of the splay-bend Ising wall that has been reported in [22]. As stressed in Section 2, the origin of this instability lies in the difference between two of the elastic constants ($K_1 > K_2$). In order to explain the instability in the vicinity of the Fréedericksz transition, we therefore need to consider that K_2 is much smaller than the other constants ($K_2 \sim \varepsilon$). Consequently the last term in the Landau equation becomes negligible. But the $Z = 0$ solution is now marginal with respect to the y-direction. In order to study the stability of the interface (where Z vanishes), the higher-order terms in the equation (4) have to be considered. With the new asymptotic limit, $Z \sim \varepsilon^{1/2}$, $\partial_y^2 \sim \mu$, $\partial_x^2 \sim \varepsilon$, $K_1 \sim K_3 \sim 1$, and $K_2 \sim \varepsilon$ (with $\varepsilon \ll \mu \ll 1$), the dynamical equation now reads

$$\begin{aligned}\gamma_1\partial_t Z = {} & \varepsilon Z - bZ^3 + \left(K_1\partial_x^2 + K_2\partial_y^2\right)Z \\ & + \frac{K_1^2}{a}\partial_{x^2y^2}Z + \frac{K_1^3}{a^2}\partial_{x^2y^4}Z - \frac{3}{4}K_3 Z\left(\partial_y Z\right)^2 \end{aligned} \tag{7}$$

with $a \equiv \epsilon_{\mathrm{a}}E^2 + K_3\pi^2/d^2$ and $\mu \equiv (K_2/\varepsilon - 2K_1/5a)$. The expression for the director can be rewritten in the following form

$$\mathbf{n} = \begin{pmatrix} n_x = Z\cos\left(\dfrac{\pi z}{d}\right) \\ n_y = \dfrac{K_1}{a}\partial_{xy}Z\cos\left(\dfrac{\pi z}{d}\right) + \dfrac{K_1^2}{a^2}\partial_{xy^3}Z\cos\left(\dfrac{\pi z}{d}\right) \\ n_z = 1 - \dfrac{Z^2}{2}\cos^2\left(\dfrac{\pi z}{d}\right) \end{pmatrix}.$$

In order to explore the instabilities of the splay-bend interface, we shall introduce the following expression:

$$Z = \sqrt{\frac{\varepsilon}{b}}\tanh\left(\sqrt{\frac{\varepsilon}{2K_1}}x - P(y)\right) + w(x,P) \tag{8}$$

where $w(x,P)$ is a small correction to the wall solution ($w \ll 1$) and P satisfies the equation below deduced from a solvability condition (see Appendix):

$$\gamma_1\partial_t P = D_1 P_{yy} + D_2 P_y^2 P_{yy} - D_3 P_{yyyy} \tag{9}$$

with $D_1 \equiv \mu\varepsilon = (K_2 - 2K_1\varepsilon/5a)$, $D_2 \equiv (48K_1^2/7)(\varepsilon/a^2)$ and $D_3 \equiv (2K_1^2/5)(\varepsilon/a^2)$.

When D_1 is positive and of order one, the preceding equation is asymptotically brought near by a diffusion equation ($\partial_t P = D_1 P_{yy}$). This is carried out in a liquid crystal sample with a weak elastic anisotropy or in a sample submitted to a strong homogeneous magnetic field ($a \gg 1$). This result is strengthened by the numerical simulations.

Experimentally, an Ising wall in a splay-bend configuration is formed in the region where the field is inhomogeneous (see Fig. 2) and then quenched into the area between the two magnets (where the field is homogeneous). Near the Fréedericksz threshold it is very difficult to maintain the wall in an averaged position between the magnets since any little imperfection on the parallelism between the sample and the plane of the magnetic field makes the wall drift towards one edge of the cell. Therefore the experiments were carried out rather far from this threshold. Starting from a wrinkled interface, one can see, for a sufficiently high magnitude of the field, the perturbations

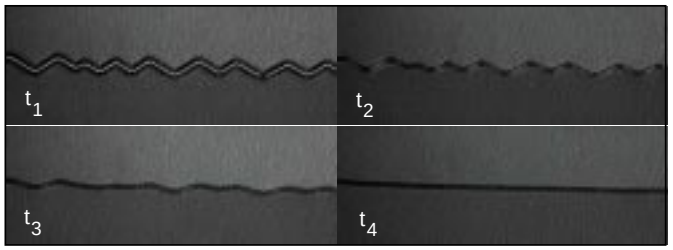

Fig. 3. Experiment of diffusive relaxation: the flat stable interface is subjected to a strong perturbation which relaxes in time without any displacement of the front ($t_1 < t_2 < t_3 < t_4$).

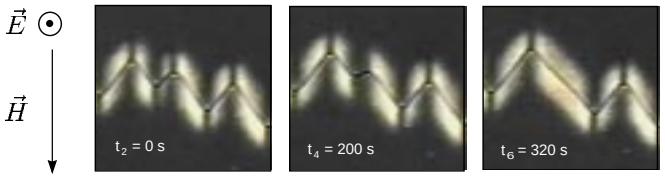

Fig. 4. Spinodal decomposition of the interface observed through a microscope with crossed polarizers.

relaxing in time (see Fig. 3). This process occurs without change in the position of the line and stops when the interface becomes straight again.

When D_1 is small (positive or negative), rescaling the space and P ($\tilde{t} \equiv t\ /\gamma_1$, $\tilde{y} \equiv y\ /\sqrt[4]{D_3}$, $\tilde{P} \equiv P\ /\sqrt{D_3/D_2}$), the asymptotic equation for P reads (omitting the tildes):

$$\partial_t P = \varepsilon P_{yy} + P_y^2 P_{yy} - P_{yyyy} \tag{10}$$

where $\varepsilon \equiv D_1/\sqrt{D_3}$, also ∂_t and ∂_y^4 are the order ε^2. The term $P_y^2 P_{yy}$ is the nonlinear diffusion, and P_{yyyy} is the hyperdiffusion. For the sake of simplicity, the signs in the latter equation have been chosen so that the nonlinear and hyperdiffusive terms saturate the instability. One must remark that the above equation is a continuity equation which expresses the conservation of the area of the $P(y)$ curve. Moreover, this is a variational equation which can be rewritten in the following form:

$$\partial_t P = -\frac{\delta \mathcal{F}}{\delta P}, \quad \mathcal{F}[P] = \int \mathrm{d}y \left\{ \varepsilon \frac{P_y^2}{2} + \frac{P_y^4}{4} + \frac{P_{yy}^2}{2} \right\} \tag{11}$$

where the "free energy" $\mathcal{F}$ depends only on the derivatives of the order parameter. Introducing the local angle $\Lambda \equiv (1/\sqrt{3})P_y$, the latter equation is reduced to:

$$\partial_t \Lambda = \partial_{yy} \left(\varepsilon \Lambda + \Lambda^3 - \Lambda_{yy} \right). \tag{12}$$

This equation is the well-known Cahn-Hilliard equation [29] which describes the phase separation dynamics in conservative systems. In the case under study here, we shall see that it accounts for the facet's separation dynamics of the interface. The latter equation does not imply equation (10) but a slightly different equation with an extra term, which is a function of time. This term can be interpreted as the interface velocity. A simple change of variable (the interface position minus the time-integral of the velocity) allows equation (10) to be reobtained. Therefore, the Cahn-Hilliard equation describes the dynamics of an interface propagating with an arbitrary velocity.

The dynamical behaviour of this equation has been studied by many authors (see for example [30,31]). This study is difficult because the functional space of the system depends on the initial condition. Actually the system has to minimize its free energy under constraint (the initial area, mass constraint)[32]. It is noteworthy that the relevant conservation law that characterizes the dynamics is

$$M = \int \Lambda \, \mathrm{d}y \tag{13}$$

and not the integral of P, owing to the translational invariance of the interface. Indeed a global translation of the interface does not affect at all its dynamical behaviour, although it changes the value of the P-integral. As a consequence this last quantity cannot characterize the dynamics.

Experimentally, the splay-bend Ising wall is unstable, when it is thrust into the homogeneous area of the magnetic field, as long as its width $\xi \approx \sqrt{2K_1 b/\varepsilon}$ is larger than a critical size. The interface first develops an instability characterized by a well-defined wavelength which is determined by the experimental parameters. Later on the sinusoidal shape of the interface becomes an angled line composed of pieces of wall turned with an angle $\pm\Psi_0$ (see Fig. 4). Two adjacent pieces, whose orientations are opposite, are connected by a region of strong curvature of the line that we shall call a "kink" [22]. The dynamics consists then in reassembling domains of even orientation, the angle of the "zig" and "zag" facets staying unchanged. This process occurs thanks to annihilations of kinks and without a characteristic lengthscale. Indeed the averaged size of the domains increases regularly in time (see Fig. 4). The dynamics, which tends to separate the zig and zag states, looks like the one-dimensional counterpart of the spinodal decomposition dynamics observed in conservative binary mixtures [29].

Understanding the loss of stability of a splay-bend Ising wall ($\varepsilon < 0$) amounts to solve the problem with a zero mass constraint as an initial condition. And indeed the dynamical behaviour deduced from the theoretical analysis is in good agreement with the experiments. From numerical simulations of equation (10), one can foresee that the interface destabilization is initialized by the appearance of a spatial modulation to a well-defined wave number ($\sqrt{-\varepsilon/2}$). Next the sinusoid is transformed into an angled line which undergoes a coarsening dynamics: the largest facets start to increase whereas, as a consequence, the shortest ones decrease and then vanish. This process yields the emergence of new periodic solutions, whose wavelength increases more and more, with a logarithmically slow growth rate [31]. The previous statement can be understood by considering the free energy

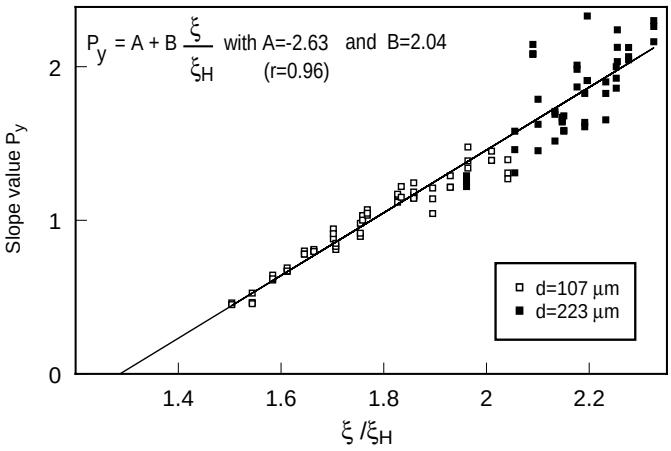

Fig. 5. Experimental curve giving the slope P_y of the interface *versus* the adimensional ratio ξ/ξ_H (ξ is the electro-magnetic coherence length and ξ_H the magnetic coherence length).

as follows: because of the zero mass constraint, the solutions that minimize the free energy satisfy the equation:

$$\Lambda_{yy} = \varepsilon\Lambda + \Lambda^3. \tag{14}$$

The spatial periodic solutions that oscillate between the two limits $\pm\sqrt{\varepsilon}$ are the local minima of $\mathcal{F}$. Nevertheless, in the presence of noise, they tend asymptotically towards the heteroclinic loop that connects the two global minima of the free energy. This accounts for the annihilation of kinks which is physically associated with the high energetic cost of the corners (Frank-Oseen free energy [25]).

The zig-zag instability of the interface is triggered by the elastic anisotropy of the liquid crystal whose influence is emphasized in the wall (which corroborates the expression of D_1). Actually, the distortions involved depend on the orientation of the interface with respect to the direction of the magnetic field. For most of the usual compounds, the energetic cost of a wall aligned with the field (twist wall) is lower than that of a wall perpendicular to the field (splay-bend wall) since $K_2 < K_1$ [27]. As a consequence, the system (splay-bend wall) reduces its energy by changing the direction of the wall. A global rotation of the interface can not happen in an infinite medium. The interface is therefore forced to rotate locally and is then divided into facets turned with an angle $\pm\Psi_0$. This angle, whose value is determined by the control parameters (see Fig. 5), results from several effects. The one which favours the rotation is the elastic effect. The other competing effects are the interface elongation along its original direction and the escape of the molecules from the vertical plane containing the magnetic field (see Fig. 1c). These two last effects disfavour the rotation. The local reorientation generates many kinks, which will disappear since they are energetically costly.

The equations (7, 9, 10) are only valid close to the Fréedericksz transition when one of the elastic constants is far smaller than the other ones ($K_2/K_1 \ll 1$). This limit actually enables us to find the "germ" of the zigzag instability (*cf.* the numerical simulation presented in Fig. 6)

Fig. 6. Numerical simulation of the equation (7) for a high anisotropy of elasticity: $K_2/K_1 = 0.056$, $K_3 = 1$, $\varepsilon = 1$, $b = 1$, $a = 1$. The picture shows the Y-component of the director in the system.

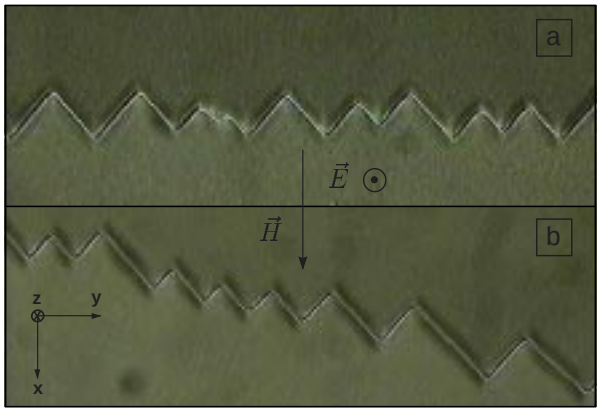

Fig. 7. Spinodal decomposition dynamics for two initial conditions: (a) interface perpendicular to the magnetic field; (b) interface slightly inclined with respect to the y-axis (direction perpendicular to the magnetic field). The polarizers are uncrossed.

and to emphasize its physical origin ($K_2 \ll K_1, K_3$). The experiments have been conversely realized far from the Fréedericksz transition and for an elastic ratio equal to $K_2/K_1 \sim 0.65$. Qualitatively the same kind of dynamical behaviour can then be observed. This indicates that the zigzag instability manifold extends far from the germ inside the parameters space. Therefore the theoretical model (10) gives a qualitative understanding of the observed physical phenomena. A similar situation is encountered in the Turing instability problem where one of the diffusion constants is assumed to be much smaller than the other one in order to account for the instability [33].

When the interface has initially a slight inclination with respect to the magnetic field, a non-zero mass constraint must be considered. The dynamical evolution is therefore similar to the latter unless there are more facets of one type than of the other (see Fig. 7b). In order to find the stationary solutions, it is convenient to introduce a Lagrange multiplier (λ), that takes into account the conserved area, and to express the free energy in the new following new form [32]:

$$\mathcal{G}[\Lambda] = \int \mathrm{d}y \left\{ \varepsilon\frac{\Lambda^2}{2} + \frac{\Lambda^4}{4} + \frac{\Lambda_y^2}{2} + \lambda\Lambda \right\}. \tag{15}$$

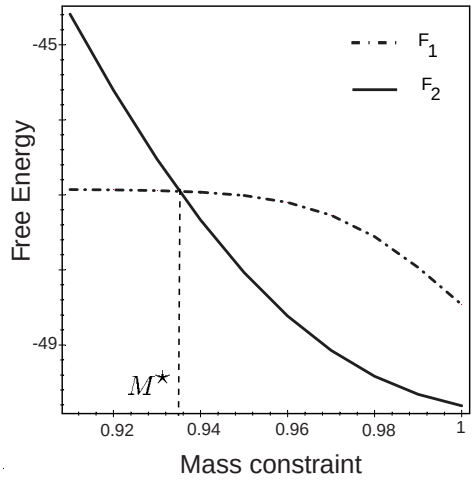

Fig. 8. Free energy value for the homoclinic solution (F_1) and for the homogeneous solution (F_2) *versus* the mass constraint ($0.92 < M < 1$).

The family of solutions that minimize this free energy now satisfies the differential equation:

$$\Lambda_{yy} = \lambda + \varepsilon\Lambda + \Lambda^3. \tag{16}$$

Obviously such solutions satisfy the equation (12). The global minimum of the free energy $\mathcal{G}$ is either the homoclinic solution (which represents an interface with three facets) or one of the homogeneous solutions, that are the local minima of the potential $V = \lambda\Lambda + \varepsilon\Lambda^2/2 + \Lambda^4/4$. One can notice that, as a consequence of the conservation law, these solutions have different Lagrange multiplier values.

If one considers a finite system with periodic boundary conditions, then it is possible to normalize the conserved quantity M with the area corresponding to the homogeneous minima of $\mathcal{F}$ ($\Lambda_{\min} = \pm\sqrt{\varepsilon}$). With respect to the mass constraint, we computed the homogeneous minimum and approximated the homoclinic solution by two heteroclinic loops (formed by two hyperbolic tangents). By evaluating the free energy $\mathcal{G}$ for these solutions, we obtained the diagram shown in Figure 8.

From this, one can deduce that, for a mass constraint M lower than about 0.94, the global minimum is given by the homoclinic solution (spinodal decomposition) whereas for M between 0.94 to 1, the global minimum is obtained with the homogeneous solution ("nucleation and growth"). Therefore the nucleation barrier is characterized by a critical area. This has been checked numerically as illustrated in Figure 9. For two slightly different initial conditions, one can observe either the spinodal decomposition or the "nucleation and growth" regime.

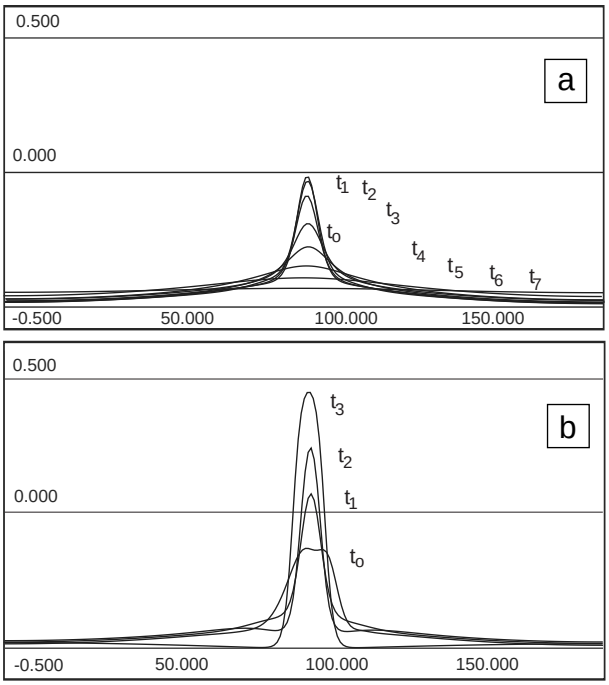

Fig. 9. Temporal evolution of a perturbation to the homogeneous state for two values of M slightly different from the critical value $M = M^\star \approx 0.94$: (a) for $M \gtrsim M^\star$, the perturbation relaxes ("nucleation and growth" regime); (b) for $M \lesssim M^\star$, it grows up ("spinodal decomposition" regime).

4 Interface under the influence of a magnetic field gradient

The curvature of the magnetic flux lines is used to produce a splay-bend Ising wall in the nematic sample. Up to now, we have considered the experimental situation where the Ising wall was afterwards thrust in the homogeneous region of the field. Differently, the Ising wall can be kept in the inhomogeneous region and the electric voltage once again decrease in order to make the interface thinner and thinner. This enhances the elastic distortions in the wall and induces its destabilization. However, for fairly strong gradients, the spinodal decomposition is no longer observable. The straight Ising wall looses its stability by evolving towards a stationary periodic configuration without annihilations of kinks (*cf.* Fig. 10). This occurs for large enough distortions, and so rather far from the Fréedericksz threshold.

The straight wall can be reobtained by decreasing further the voltage, which means that the effective control parameter of the instability depends nonlinearly on the electric field. This is qualitatively what is found from the theoretical model (see the expression of D_1 which is quadratic in the electric field).

In order to consider the prevailing effect of the magnetic field gradient, one must add an extra term in the equation (7), that now reads

$$\begin{aligned}\gamma_1\partial_t Z = {} & \varepsilon Z - bZ^3 + \left(K_1\partial_x^2 + K_2\partial_y^2\right) Z \\ & + \frac{K_1^2}{a}\partial_{x^2y^2} Z + \frac{K_1^3}{a^2}\partial_{x^2y^4} Z \\ & - \frac{3}{4}K_3 Z\left(\partial_y Z\right)^2 + \frac{8\gamma H_z(x)}{\pi H}\end{aligned} \tag{17}$$

where $H_z(x)$ is the component of the magnetic field in the vertical direction and $\gamma \equiv (1/2)\chi_{\rm a}H^2$. The term

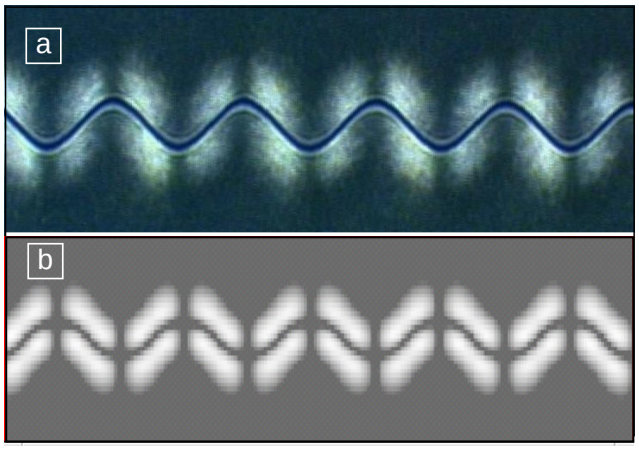

Fig. 10. Influence of a magnetic field gradient on the instability: (a) experimental photograph; (b) picture from a numerical simulation of the equation (17) ($K_2/K_1 = 0.021$, $K_3 = 1$, $\varepsilon = 1$, $b = 1$, $a = 1$, $(8\gamma/\pi)(\Delta H/H) = -0.6$).

accounting for the vertical magnetic field in equation (17) is assumed to be of order $\mu^2\varepsilon^{3/2}$. For the sake of simplicity, we moreover suppose that the function $H_z(x)$ is well-approximated by a linear function ($H_z(x) = -(\Delta H/L)x$). Starting from this, we find the following equation for the interface:

$$\partial_t P = -\lambda P + \varepsilon P_{yy} + P_y^2 P_{yy} - P_{yyyy} \qquad (18)$$

where $\lambda = (12\sqrt{2}/\pi)(\gamma\Delta H/L\varepsilon^{1/2})$ (the derivation has been done in the same way as shown in the Appendix). The magnetic field gradient breaks the translational symmetry of the interface ($P \to P + P_0$). The linear stability analysis of the homogeneous solution displays an instability to the wave number ($\sqrt{-\varepsilon/2}$) when $\lambda = -\varepsilon^2/4$. Experimentally the interface behaviour strongly resembles the latter prediction (*cf.* Fig. 10a) which is moreover corroborated by the numerical simulations of equation (17) (see Fig. 10b).

The magnetic field gradient generates a drift of the interface towards a homogeneous equilibrium position ($P = 0$). For a splay-bend Ising wall lying along this direction, the molecules follow almost everywhere the magnetic flux lines. This minimizes the energetic term associated with the magnetic interaction. The gradient acts therefore as a restoring force around a particular position. It stabilizes the straight splay-bend configuration of the wall and, beyond the instability threshold, saturates the amplitude of the zig-zag line. Thus the magnetic field gradient is an antagonistic effect to the elastic anisotropy which triggers the instability. If $H_z(x)$ were an asymmetric function, it would generate an extra constant term in the interface equation. This one represents the new homogeneous equilibrium position ($P = P_0$).

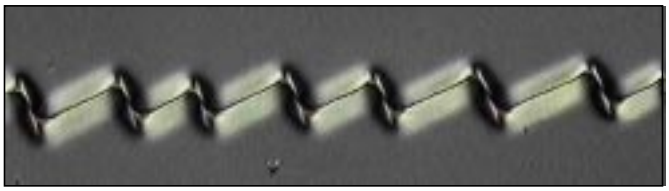

Fig. 11. Experimental photograph of an unstable interface in a cholesteric sample.

5 Zig-zag instability in cholesteric liquid crystal

The cholesteric phase differs from the nematic one in its lowest energy distribution of directors which is an helicoidal, and not uniform, distribution. The cholesteric phase is thus characterized by a "natural" tendency to the twist distortion (in a specified sense of rotation). In the specific problem under study, this leads to the lack of reflection symmetry with respect to the vertical plane [25]. In the Frank free energy, this results in a new term which expresses the rolling tendency of the cholesteric phase that quantifies the chirality (Q_0) of the material [34].

We have carried out again experiments but with a cholesteric compound this time. More precisely we used 5CB in which we added a small amount of chiral compound (ZLI-811 from Merck). The width of the cell has been chosen at least twice as small as the helicoidal pitch of the cholesteric phase. In this new situation, the observed instability is quite similar to the nematic one. The spinodal decomposition and the coarsening dynamics are still visible. Nevertheless, the facets are no longer symmetric. One kind of facet is actually more tilted than the other one with respect to the magnetic field (see Fig. 11). This can be easily explained from an elastic point of view. Indeed, when the splay-bend Ising wall becomes unstable, the distortions involved in the wall change in order to decrease the energy. Some twist distortions replace partially the initial pure splay distortion (see Fig. 1c). For one kind of facet, this twist distortion is similar to the distortion naturally favored by the cholesteric phase. Conversely, the other one is disfavored by the chirality. This produces a dissymmetry, the largest facets corresponding to the favoured twist.

In order to take into account the chirality, we have to add the term $Q_0\left(\boldsymbol{\nabla}\times\mathbf{n} - \mathbf{n}\left(\mathbf{n}\cdot\boldsymbol{\nabla}\times\mathbf{n}\right)\right)$ in the director equation (3). The additional term leads to the following corrections to the equation (7):

$$\begin{aligned}\gamma_1\partial_t Z = {} & \varepsilon Z - bZ^3 + \left(K_1\partial_x^2 + K_2\partial_y^2\right)Z \\ & + \frac{K_1^2}{a}\partial_{x^2y^2}Z + \frac{K_1^3}{a^2}\partial_{x^2y^4}Z - \frac{3}{4}K_3 Z\left(\partial_y Z\right)^2 \\ & + \chi\frac{K_1}{a}\left(2\partial_x Z\,\partial_{xy}Z + \partial_y Z\,\partial_{xx}Z\right) \\ & + \chi\frac{K_1^2}{a^2}\partial_y^2\left(2\partial_x Z\,\partial_{xy}Z + \partial_y Z\,\partial_{xx}Z\right) \\ & + \chi\frac{K_1^2}{a^2}\partial_{xy}\left(\partial_{xy}Z\,\partial_y Z\right) \qquad (19)\end{aligned}$$

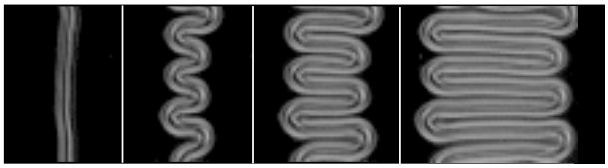

Fig. 12. Destabilization of a cholesteric "finger".

where $\chi \equiv (16/3)Q_0$. In order to analyze the instability of the splay-bend interface, one must therefore consider that the terms proportional to the chirality are only perturbative ones ($Q_0 \ll 1$). From the persistence condition of the splay-bend wall, one can obtain the following equation for the interface (after renormalization):

$$\partial_t P = \varepsilon P_{yy} + \varepsilon^{\frac{1}{2}} \alpha P_y P_{yy} + P_y^2 P_{yy} - P_{yyyy} \qquad (20)$$

where $\alpha \equiv (11/2)(\chi\ K_1^2/a^2\sqrt{D_2}\sqrt[4]{D_3})$. Such an equation can be rewritten in the same form as equation (10) by using the simple change of variable $\tilde{P} \equiv P + \varepsilon^{1/2}\alpha y/2$. However, the influence of the chirality on the interface dynamics is more obvious from the latter one. The main effect of the chirality over the interface is to make the facets asymmetric. These differ in slope by $\varepsilon^{1/2}\alpha/2$. The additional term $\varepsilon^{1/2} P_y P_{yy}$ is asymptotically negligible with respect to the other ones. This term actually derives from the two last terms of equation (19), which are also asymptotically negligible. This explains that a strong asymmetry in the facets cannot be observed numerically although it exists experimentally. However this term expresses quite well the qualitative influence of the chirality.

Lastly, a new dynamical behaviour for the interface equation is expected when the nonlinear term does not saturate the instability ($-P_y^2 P_{yy}$) so that the interface increases indefinitely. Such a phenomenon has not been observed on Ising walls but is visible on cholesteric fingers as it is shown in Figure 12. These can be modelled as walls connecting two identical states. This work is in progress and we hope to report on this in the future.

6 Conclusion

In summary, we have experimentally and theoretically investigated the dynamical behaviour of an Ising wall formed in a nematic or cholesteric liquid crystal subjected to external magnetic and electric fields. When the straight interface is stable, its behaviour under perturbations obeys a diffusion equation (*cf.* Fig. 2). For small diffusion coefficient, the system must be modelled by the more complex equation (10). This one accounts for the zig-zag instability experimentally observed and for the facets dynamics that follows (*cf.* Fig. 6). Apart from symmetry arguments, it can be deduced from the theory of the elasticity of the liquid crystals assuming that all the relevant phenomena occur in the vicinity of the Fréedericksz transition. Under this assumption, we have deduced the Landau equation which describes the appearance of orientation domains but only allows the existence of stable interfaces. In order to account for the splay-bend Ising wall instability, we must consider that one of the elastic constants (K_2) is far smaller than the others. This makes the dynamics richer; this one is now asymptotically brought near by equation (7) that provides a good understanding of the physical phenomena. The variational equation (10) for the interface position can then be derived from the previous equation. Its gradient is a one-dimensional Cahn-Hilliard equation. It has to be modified in order to model the influence of slightly broken symmetries in the system. The lack of translational symmetry, experimentally realized by applying a magnetic field gradient, gives rise to an instability of a well-defined wave number. It is expressed thanks to a constant and a linear term in the interface equation (18). In the case of a cholesteric liquid crystal, the zig-zag instability induces an asymmetric faceting of the interface. In this case actually, the system does not contain the reflection symmetry in the direction tangential to the interface. As a consequence, two adjacent facets are no longer symmetric, which is expressed in equation (20) by the new term $P_y P_{yy}$.

The asymptotic limit used in the theoretical analysis has been chosen in order to emphasize the influence of the elastic anisotropy ($K_2 \sim \varepsilon$). Such a limit seems actually essential to account for the experimental observations, and indeed it allows a quite good description of the physical phenomena experimentally observed.

The authors would like to thank M. Nobili for experimental collaboration and S. Thiberge for fruitful discussions. One of us (P.C.) thanks the support of the "Institut Universitaire de France". The simulation software developed at the laboratory INLN in France has been used for all the numerical simulations presented in this paper.

Appendix

Putting the ansatz (8) in the equation (7) and linearizing this latter with respect to w, we found:

$$\begin{aligned}\mathcal{L}w = {} & \gamma_1 \partial_t P(\partial_{x_0} Z_0) - P_{yy}(\partial_{x_0} Z_0) + P_y^2(\partial_{x_0}^2 Z_0) \\ & + \frac{K_1\varepsilon}{2a}\left[-P_{yy}\ (\partial_{x_0}^3 Z_0) + P_y^2(\partial_{x_0}^4 Z_0)\right] \\ & + \frac{K_1^2\varepsilon}{2a^2}\left[-P_{yyyy}\ (\partial_{x_0}^3 Z_0) + 4P_y\ P_{yyy}(\partial_{x_0}^4 Z_0)\right. \\ & \left. + 3P_{yy}^2(\partial_{x_0}^4 Z_0) - 6P_y^2 P_{yy}(\partial_{x_0}^5 Z_0) + P_y^4(\partial_{x_0}^6 Z_0)\right] \\ & - \frac{3}{4}K_3 P_y^2\ Z_0(\partial_{x_0} Z_0)^2 \end{aligned} \qquad (A.1)$$

with

$$Z_0 = \sqrt{\frac{\varepsilon}{b}}\tanh\left(\sqrt{\frac{\varepsilon}{2K_1}}x - P\right),$$
$$x_0 = \sqrt{\frac{\varepsilon}{2K_1}}x - P$$

and

$$\mathcal{L} = -\left(\varepsilon - 3bZ_0^2 + K_1\partial_x^2\right).$$

$\mathcal{L}$ is an Hermitian operator with respect to the scalar product $\langle fg \rangle = \int_{-\infty}^{+\infty} fg \, \mathrm{d}x$. Moreover the adjoint operator $\mathcal{L}^\dagger$ possesses a Goldstone mode corresponding to the translational invariance ($\mathcal{L}^\dagger(\partial_{x_0} Z_0) = 0$). Then (A.1) has a solution w if its right-hand side is orthogonal to the kernel of $\mathcal{L}^\dagger$, *i.e.* is orthogonal to $(\partial_{x_0} Z_0)$ (Fredholm alternative). The previous condition leads to the equation (9). It is noteworthy that, because Z_0 is an odd function of x_0, the scalar products $\langle \partial_{x_0} Z_0 \mid \partial_{x_0}^2 Z_0 \rangle$, $\langle \partial_{x_0} Z_0 \mid \partial_{x_0}^4 Z_0 \rangle$, $\langle \partial_{x_0} Z_0 \mid \partial_{x_0}^6 Z_0 \rangle$ and $\langle \partial_{x_0} Z_0 \mid Z_0 (\partial_{x_0} Z_0)^2 \rangle$ vanish. Then the only relevant terms in equation (9) are proportional to P_{yy}, $P_y^2 P_{yy}$ and P_{yyyy}.

References

1. J.S. Langer, Rev. Mod. Phys. **52**, 1 (1980) and references therein.
2. *Growth and Form - Non Linear Aspects*, edited by M. Ben Amar *et al.* (Plenum Press, New York, 1991).
3. W.W. Mullins, R.F. Sekerka, J. Appl. Phys. **35**, 444 (1964).
4. M.E. Glicksman, R.J. Shaefer, J.D. Sayers, Metall. Trans. A **7**, 1747 (1976); J.S. Langer, R.F. Sekerka, T. Fujioka, J. Cryst. Growth **44**, 414 (1978).
5. J.S. Langer, H. Müller-Krumbhaar, Acta Metall. **26**, 1681 (1978); R.C. Brower, D.A. Kessler, J. Koplik, H. Levine, Phys. Rev. A **29**, 1335 (1984); D.A. Kessler, H. Levine, Phys. Rev. Lett. **57**, 3069 (1986).
6. S. Cheveigné, C. Guthmann, M.M. Lebrun, J. Phys. France **47**, 2095 (1986); S. de Cheveigné, C. Guthmann, P. Kurowski, E. Vicente, H. Biloni, J. Cryst. Growth **92**, 616 (1988); J. Bechhoefer, A.J. Simon, A. Libchaber, P. Oswald, Phys. Rev. A **40**, 2042 (1989).
7. C. Misbah, H. Müller-Krumbhaar, Y. Saito, D.E. Temkin, in *Growth and Form*, edited by M. Ben Amar (Plenum Press, New York, 1991).
8. C. Misbah, A. Valance, Phys. Rev. E **49**, 166 (1994).
9. A. Novick-Cohen, Physica D **26**, 403 (1987).
10. P. Pelcé, A. Pumir, J. Cryst. Growth **73**, 337 (1985).
11. P.G. Saffman, G.I. Taylor, Proc. R. Soc. Lond. A **245**, 312 (1958); J.W. Mc Lean, P.G. Saffman, J. Fluid. Mech. **102**, 455 (1981).
12. J. Bechhoefer, in *Spatio-temporal Patterns in Nonequilibrium Complex Systems*, edited by P.E. Cladis, P. Palffy-Muhoray (Addison-Wesley Publishing Company, 1994).
13. J. Burgers, Adv. Appl. Mech. **1**, 171 (1948).
14. Y. Kuramoto, T. Tsuzuki, Prog. Theor. Phys. **55**, 356 (1976).
15. G.I. Sivashinsky, Acta Astronautica **4**, 1177 (1977).
16. P. Clavin, Prog. Energy Combust. Sci. **11**, 1 (1985); P. Pelcé, P. Clavin, J. Fluid. Mech. **124**, 219 (1982); F. Sabathier, L. Boyer, P. Clavin, Prog. Astro. Aeronautics **76**, 246 (1981); G.I. Sivashinsky, Ann. Rev. Fluid. Mech. **15**, 179 (1983).
17. C. Misbah, H. Müller-Krumbhaar, D.E. Temkin, J. Phys. I France **1**, 585 (1991).
18. A.A. Golovin, S.H. Davis, A.A. Nepomnyashchy, Physica D **122**, 202 (1998).
19. Y. Pomeau, A. Pumir, P. Pelcé, J. Stat. Phys. **37**, 39 (1984); P. Manneville, in *Propagation in Systems Far from Equilibrium*, edited by J.E. wesfreid *et al.* (Springer-Verlag, Berlin, 1988).
20. Y. Kuramoto, in *Chemical Oscillations, Waves and Turbulence*, Synergetics 19 (Springer, Berlin, 1984).
21. A.J. Simon, J. Bechhoefer, A. Libchaber, Phys. Rev. Lett. **61**, 2574 (1988).
22. C. Chevallard, M. Clerc, P. Coullet, J.-M. Gilli, Phys. Rev. Lett. (submitted); C. Chevallard, M. Nobili, J.-M. Gilli, Liquid Crystals (to be published).
23. P. Manneville, J.-M. Piquemal, Phys. Rev. A **28**, 1774 (1983); M.C. Cross, P.C. Hohenberg, Rev. Mod. Phys. **65** (1993).
24. R. Ribotta, A. Joets, Lin Lei, Phys. Rev. Lett. **56**, 1595 (1986); E. Bodenschatz, M. Kaiser, L. Kramer, W. Pesch, A. Weber, W. Zimmermann, in *New Trends in Nonlinear Dynamics and Pattern-Forming Phenomena*, edited by P. Coullet, P. Huerre (Plenum Press, New York, 1990).
25. P.G. de Gennes, J. Prost, *The physics of Liquid Crystals*, 2nd edn. (Oxford Science Publications, Clarendon Press, 1993).
26. W. Helfrich, Phys. Rev. Lett. **21**, 1518 (1968).
27. F. Brochard, J. Phys. France **33**, 607 (1972).
28. L.N. Bulaevskii, V.L. Ginzburg, Zh. Eksp. Teor. Fiz. **45**, 772 (1963) [Sov. Phys. JETP, **18**, 530 (1964)]; P. Coullet, J. Lega, B. Houchmanzadeh, J. Lajzerowicz, Phys. Rev. Lett. **65**, 1352 (1990); J.-M. Gilli, M. Morabito, T. Frisch, J. Phys. II France **4**, 319 (1994).
29. J.W. Cahn, J.E. Hilliard, J. Chem. Phys. **28**, 258 (1958).
30. T. Kawasaki, T. Munakata, Prog. Theor. Phys. **74**, 656 (1988); T. Kawasaki, T. Ohta, Physica A **11**, 573 (1982).
31. N. Alikakos, P.W. Bates, G. Fusco, J. Diff. Eqs. **90**, 81 (1990); P.W. Bates, J.P. Xun, J. Diff. Eqs. **111**, 421 (1990).
32. C.M. Elliot, D. French, IMA J. Appl. Math. **38**, 97 (1987); J.C. Eilbeck, J.E. Furter, M. Grinfeld, Phys. lett. A **135**, 272 (1989).
33. A. Turing, Philos. Trans. Roy. Soc. Lond. **237**, 37 (1952).
34. L.D. Landau, in *Statistical Physics 1*, edited by L.D. Landau, D. Lifschitz (Pergamon Press edition, 1990).